ACS APPLIED MATERIALS & INTERFACES

Research Article

www.acsami.org

Targeting Chemophotothermal Therapy of Hepatoma by Gold Nanorods/Graphene Oxide Core/Shell Nanocomposites

Cheng Xu, Darong Yang, Lin Mei, Qiuhong Li,* Haizhen Zhu,* and Taihong Wang*

Key Laboratory for Micro-Nano Optoelectronic Devices of Ministry of Education and State Key Laboratory for Chemo/Biosensing and Chemometrics, Collage of Biology, Hunan University, Changsha, 410082, People's Republic of China

Supporting Information

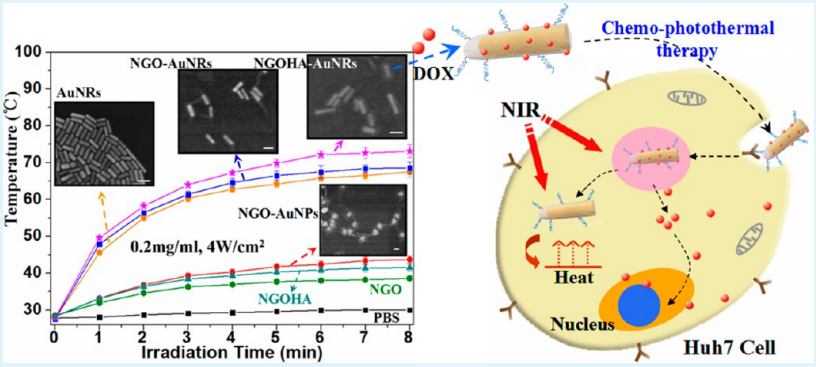

ABSTRACT: Nanographene oxide (NGO) are highly suitable to be the shells of inorganic nanomaterials to enhance their biocompatibility and hydrophilicity for biomedical applications while retaining their useful photonic, magnetic, or radiological functions. In this study, a novel nanostructure with gold nanorods (AuNRs) encapsulated in NGO shells is developed to be an ultraefficient chemophotothermal cancer therapy agent. The NGO shells decrease the toxicity of surfactant-coated AuNRs and provide anchor points for the conjugation of hyaluronic acid (HA). The HA-conjugated NGO-enwrapped AuNR nanocomposites (NGOHA-AuNRs) perform higher photothermal efficiency than AuNRs and have the capability of targeting hepatoma Huh-7 cells. NGOHA-AuNR is applied to load doxorubicin (DOX), and it exhibits pH-responsive and near-infrared light-triggered drug-release properties. Chemophotothermal combined therapy by NGOHA-AuNRs-DOX performs 1.5-fold and 4-fold higher targeting cell death rates than single chemotherapy and photothermal therapy, respectively, with biosafety to nontargeting cells simultaneously. Furthermore, our strategy could be extended to constructing other NGO-encapsulated functional nanomaterial-based carrier systems.

KEYWORDS: *graphene oxide, gold nanorods, core/shell materials, drug delivery, photothermal therapy, cancer therapy*

1. INTRODUCTION

Chemotherapy, one of the most commonly used cancer therapeutic approaches, shows many limitations, such as systemic side effects, low efficacy, and drug resistance.[1] To enhance anticancer efficacy and optimize therapy, integration of multiple treatment strategies with synergistic effects is highly expected.[2] The use of nanomaterials in medicine offers the capability of combining multiple therapeutic methods in a single carrier system.[3] Various functional nanomaterials such as gold nanoparticles (AuNPs),[4,5] semiconductor quantum dots,[6,7] carbon nanomaterials,[8] and magnetic nanoparticles[3,9] have been investigated to combine multiple therapeutic approaches [e.g., imaging, gene therapy, and photothermal therapy (PTT)] with chemotherapy. Among these treatment strategies, the combination of PTT with chemotherapy, termed chemophotothermal therapy, as a minimally invasive, controllable, and highly efficient treatment method, has drawn widespread attention.[10,11]

To avoid nonspecific heating and enable deeper penetration into biological tissues, photothermal agents must show high absorption in the near-infrared (NIR) region and selective uptake by cancer cells.[12,13] Noble-metal nanomaterials, especially gold nanorods (AuNRs), have shown great potential in targeted photothermal cancer therapy and drug delivery.[14−17] However, the only use of AuNRs has several disadvantages because cetyltrimethylammonium bromide (CTAB) has been widely used as a surfactant in the synthesis of AuNRs, but it is toxic to cells and difficult to remove completely.[18] In addition, CTAB-coated AuNRs lack cancer-targeting and drug-loading capability. Therefore, controlled surface modification of AuNRs is of critical importance.

Graphene oxide (GO), a two-dimensional layer of carbon nanomaterial, has attracted remarkable attention in the areas of drug and gene delivery,[19−21] protein delivery,[22] and imaging in vitro.[23] GO possesses unique features such as facile synthesis,

Received: August 21, 2013
Accepted: November 25, 2013
Published: November 25, 2013

prominent flexibility, abundant functional groups on the surface, and good biocompatibility both in vitro and in vivo,[24−27] which make it highly suitable to be shell materials for the surface modification of nanomaterials. Sreejith et al.[28] encapsulated dye-loaded mesoporous silica nanoparticles in GO nanosheets, and they found that GO shells were very stable and could be protective vessels for preventing dye leakage. Chen et al.[29] demonstrated that unifunctional nanoparticles can be wrapped by graphene in a nonchemically specific manner to produce multifunctional structures without the need for complex multistep chemical synthesis. In our previous study,[30] the encapsulation of nanographene oxide (NGO)[23] not only decreased the cytotoxicity of CTAB-coated AuNRs but also provided anchor points on AuNRs for further modification. The fabrication of NGO-encapsulated AuNRs is a simpler and low-cost assembly process compared with conjugating surface ligands[31] and the silica-encapsulation[17] strategy. On the other hand, NGO with appropriate polymer conjugation (e. g., PEGylated NGO, pluronic coated NGO) could be a potential NIR photothermal agent, as illustrated by in vivo experiments.[32,33] More recently, some groups reported that gold nanostructures with GO or reduced GO hybrids had high photothermal energy conversion efficiency.[34,35] Therefore, it is reasonable to expect that polymer-conjugated NGO shells will enhance the PTT efficiency of AuNRs.

Hyaluronic acid (HA) is a biocompatible, biodegradable, nonimmunogenic, and linear polysaccharide, which has shown great potential in a variety of biomedical applications, including drug delivery,[36] bioimaging,[37] and antivirus treatment.[38] HA receptors such as the hyaluronan receptor for endocytosis and cluster determinant 44 (CD44) have been exploited as target sites for HA-based drug-delivery systems. Kim et al.[37] conjugated HA derivatives to quantum dots to assess the possibility of HA derivatives as target-specific drug-delivery carriers to liver tissues. They found that the HA-based drug-delivery system could more efficiently deliver to hepatic stellate cells and hepatoma cells than normal hepatocytes. More recently, Li et al.[39] designed a HA−GO conjugate system for cancer-targeted photodynamic therapy. The conjugation of biocompatible and hydrophilic HA on GO nanosheets not only enhanced the solubility of GO in physiological conditions but also offered the capability of targeting cancer cells with HA receptors.

In this work, we report the novel design of a chemophotothermal therapy nanocarrier by encapsulating AuNRs in NGO through electrostatic self-assembly between negatively charged NGO and positively charged AuNRs. In the resulting NGO-encapsulated AuNR nanocomposites (NGO-AuNRs), ultrathin NGO shells effectively enwrapped most of the individual AuNRs with excellent dispersibility. Adipic acid dihydrazide (ADH)-modified HA (HA-ADH) was then conjugated onto the surface of NGO-AuNRs through an amide linkage. Doxorubicin (DOX) used as an example of an anticancer drug was finally loaded on HA-conjugated NGO-enwrapped AuNR nanocomposites (NGOHA-AuNRs) by $\pi-\pi$-stacking and hydrophobic interactions. This unique design could improve the interfacial properties of AuNRs and integrate the advantages of PTT agents and drug-delivery carriers. These advantages include the following: (1) Encapsulation by NGO shells decreased the toxicity of CTAB-coated AuNRs and provided anchor points for HA. (2) HA modification improved the solubility and dispersity of NGO-AuNRs in physiological conditions and targeted toward hepatoma cells. (3) The presence of HA-conjugated NGO (NGOHA) shells enhanced the photothermal effects of AuNRs. As a consequence, it was found that DOX-loaded NGOHA-AuNRs as a multifunctional vector presented high chemophotothermal therapy efficiency to hepatoma Huh-7 cells with biosafety to the normal cells.

2. MATERIALS AND METHODS

2.1. Materials. Native graphite flake was purchased from Alfa Aesar. Sodium hyaluronate, the sodium salt of hyaluronic acid (HA), with a molecular weight of 10 kDa was purchased from Shanghai Kayon Biological Technology Co. Ltd.; *N*-hydroxysuccinimide (NHS), *N*-[3-(dimethylamino)propyl]-*N*′-ethylcarbodiimide hydrochloride (EDC), adipic acid dihydrazide (ADH), doxorubicin hydrochloride (DOX), and 1-hydroxybenzotrizole (1-HoBt) were purchased form Aladdin Chemistry Co. Ltd.; $HAuCl_4$, $AgNO_3$, $NaBH_4$, and cetyltrimethylammonium bromide (CTAB) were purchased from Sinopharm Chemical Reagent Co. Ltd., China; [3-(4,5-dimethylthiazol-2-yl)-3,5-diphenytetrazolium bromide] (MTT) was purchased from Sigma-Aldrich Co. Ltd.; Dulbecco's modified Eagle's medium (DMEM) was purchased from Invitrogen Co. Ltd.; other chemicals mentioned in this article were purchased from Sinopharm Chemical Reagent Co. Ltd., China, with analytical grade and used as received. Milli-Q water was used in all experiments.

2.2. Preparation of NGO-AuNRs. GO was prepared by a modified Hummer's method.[40] The obtained GO was converted to carboxylated GO (GO-COOH)[23] and then exfoliated into NGO by repetitive strong sonication and high-speed centrifugation.[30,41] AuNRs were synthesized according to the seed-mediated growth method with the surfactant CTAB.[14] For comparison, Au nanoparticles were also prepared.[30] NGO-AuNRs were fabricated via an electrostatic interaction reported in our previous work.[30] In a typical process, 5 mL of a AuNR aqueous dispersion (1.4 mg/mL) was added into a 30 mL aqueous nGO suspension (0.05 mg/mL) and mildly stirred for 1 h. GO-AuNRs were obtained by centrifugation (8000 rpm for 10 min) and redispersed in deionized (DI) water.

2.3. Preparation of NGOHA-AuNRs. HA-ADH was synthesized as described elsewhere.[39] In brief, HA (0.05 g) was dissolved in DI water (20 mL), and then ADH (0.1 g) was added. The pH was adjusted to 6.8. Then EDC (0.05 g) and 1-HoBt (0.07 g) were added, and the resulting solution was stirred overnight. The product was transferred to the dialysis tubing (MWCO = 1 kDa) and dialyzed against 100 mM NaCl for 2 days and DI water for 2 more days. HA-ADH was obtained by freeze-drying. HA-ADH was conjugated to NGO-AuNRs through an amide bond in the presence of EDC and NHS. In a typical procedure, an aqueous solution of HA-ADH (25 mg) and EDC (0.025 g) was added to the NGO-AuNR solution (0.5 mg/mL, 20 mL). After stirring for 30 min, additional EDC (0.07 g) and NHS (0.11 g) were added, and the resulting solution was stirred overnight. After the reaction was terminated, NGOHA-AuNRs were obtained by centrifugation (8000 rpm for 15 min) and redispersed in DI water. Finally, the collected solid was redispersed and dialyzed (MWCO = 14 kDa) against distilled water for 5 days, and it formed a stable dark-green solution (about 1.2 mg/mL NGOHA-AuNRs).

2.4. Characterization. The samples were characterized by scanning electron microscopy (SEM; Hitachi S-4800) and transmission electron microscopy (TEM; JEM-2100F, 200 kV).^{1}H NMR analysis was performed by a nuclear magnetic resonance spectrometer (INOVA-400, Varian Co. Ltd.) in D_2O. The UV−vis absorption spectra were recorded by a UV1601 spectrometer (Shimadzu Co. Ltd.). The samples for Fourier transform infrared (FT-IR) testing were prepared in KBr pellets. Thermogravimetric analysis (TGA) data were achieved on a Netzsch STA449C in O_2 and N_2 atmospheres, respectively, at a heating rate of 10 °C/min from 30 to 800 °C. Dynamic light scattering (DLS) and ζ potential analysis were performed using a Malvern Zetasizer Nano 3000 HS (Malvern, Worcestershire, England).

2.5. Photothermal Effect of NGOHA-AuNRs. NGO, NGOHA, AuNRs, NGO-AuNRs, NGO-enwrapped AuNPs (NGO-AuNPs), and NGOHA-AuNRs in a phosphate-buffered saline (PBS) solution were irradiated by NIR laser (808 nm, power density = 4 W/cm^2) for different time periods to determine the photothermal energy conversion

Figure 1. Schematic illustration for the synthesis of NGOHA-AuNRs-DOX and the possible mechanism in targeted chemophotothermal therapy to hepatoma Huh-7 cells.

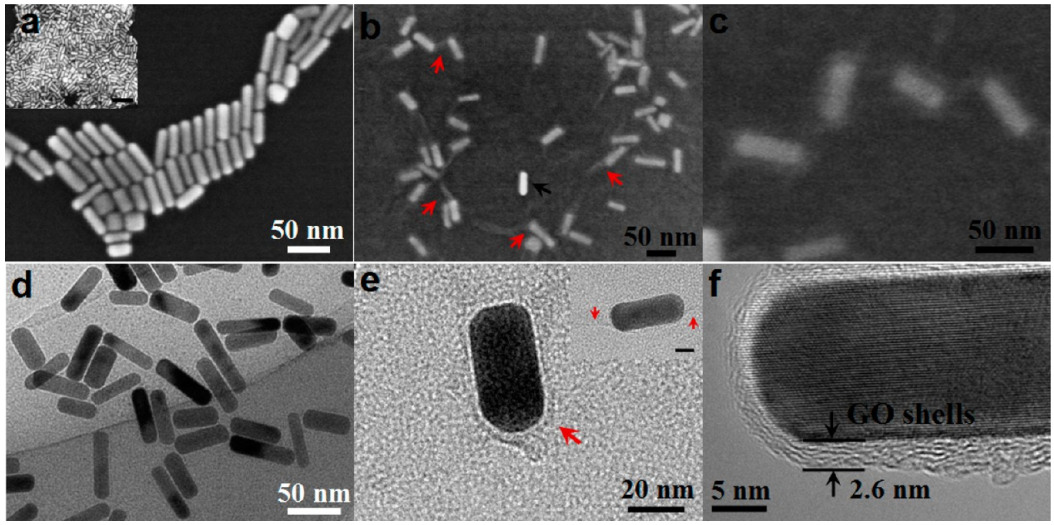

Figure 2. Morphology and structure of AuNRs, NGO-AuNRs, and NGOHA-AuNRs, SEM images of AuNRs (a), NGO-AuNRs (b), and NGOHA-AuNRs (c), TEM images of AuNRs (d) and NGO-AuNRs (e), and HRTEM image of NGO-AuNRs (f). The red arrows pointed to the presence of the redundant NGO shells, and the black arrow pointed to AuNRs without encapsulation of NGO. The scale bars of the insets in parts a and e were 200 and 10 nm, respectively.

efficiency. The AuNR concentration in NGO-AuNRs and NGOHA-AuNRs was the same as that of AuNRs. To study the impact of the NIR power density and material concentrations on the photothermal heating effect, NGOHA-AuNRs with different concentrations were irradiated under different power densities. The solution temperature was recorded by a thermometer.

2.6. DOX Loading and Release. DOX was loaded on NGOHA-AuNRs by mixing the drug with NGOHA-AuNRs in a PBS buffer at different pH values (5.3, 6.0, and 7.4) overnight, and the excessive or unbound DOX was left in the supernatant after centrifugation. The DOX concentration in the supernatant was recorded to calculate the loading efficiency. In the release experiments, NGOHA-AuNRs-DOX in PBS at different pH values (5.3, 6.0, and 7.4) were loaded into dialysis tubes of 8 kDa MWCO. At each time point, the NGOHA-AuNRs-DOX solution was irradiated by a NIR laser (4 W/cm^2) for 5 min. Each of 0.5 mL dialysis solutions was removed before and after NIR stimulation, and the same volume of fresh corresponding buffer was added back in. The amount of released DOX was measured by UV−vis at a wavelength of 490 nm.

2.7. Cell Culture and Cellular Uptake of NGOHA-AuNRs-DOX. Hepatoma Huh-7 cells[42] and Chinese Hamster Ovary (CHO) cells were grown in DMEM supplemented with 10% fetal bovine serum, L-glutamine, nonessential amino acid, penicillin, and streptomycin. Cells were seeded in tissue culture flasks (about 3 × 10^5 cells) and incubated in a fully humidified atmosphere at 37 °C with 5% CO_2.

To observe the cellular uptake of NGOHA-AuNRs-DOX, Huh-7 cells were seeded into 24-well plates in 1 mL of DMEM-containing antibiotics for 12 h. DMEM-containing free DOX and NGOHA-AuNRs-DOX were added to cells. The amounts of DOX in NGOHA-AuNRs-DOX and free DOX were 10 μg. After incubation for 1, 3, 6, 12, and 24 h, the cells were washed by PBS and observed by a

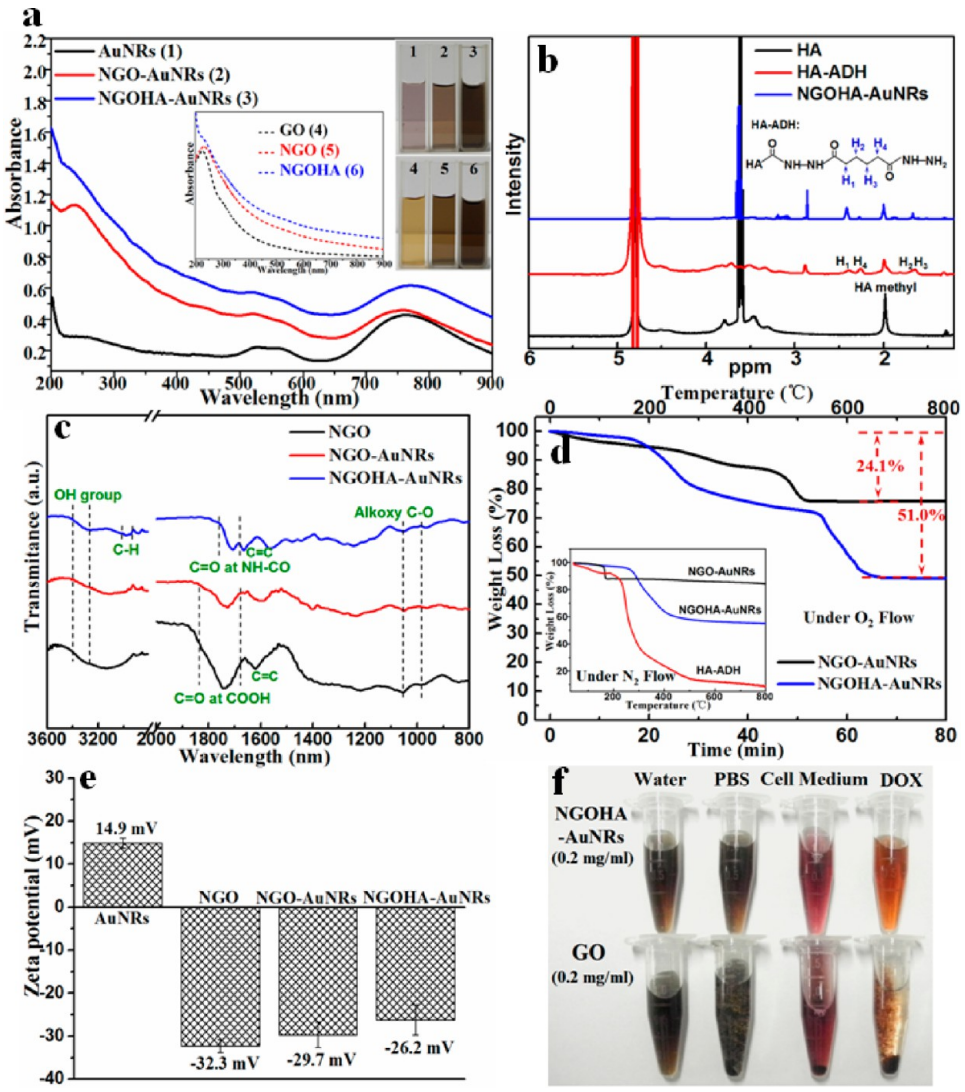

Figure 3. (a) UV−vis absorption spectra and photographs (inset) of AuNRs, NGO-AuNRs, and NGOHA-AuNRs. Inset: UV−vis absorption spectra and photographs of GO, NGO, and NGOHA. (b) ^{1}H NMR spectra of HA polymers, HA-ADH, and NGOHA-AuNRs in D_2O. (c) FT-IR spectra of NGO, NGO-AuNRs, and NGOHA-AuNRs. (d) TGA curves of NGO-AuNRs and NGOHA-AuNRs under O_2 flow and analysis curves of HA-ADH, NGO-AuNRs, and NGOHA-AuNRs under N_2 flow (inset) at a heating rate of 10 °C/min. (e) ζ potentials of NGO, AuNRs, NGO-AuNRs, and NGOHA-AuNRs. (f) Digital images of NGOHA-AuNRs and GO (0.2 mg/mL) dispersed in water, PBS, cell medium, and DOX solution (0.5 mg/mL).

fluorescence microscope (Olympus IX71; the red filter set was used for DOX imaging; excitation/emission = 545 nm/620 nm).

Quantitative measurements of the cellular uptake of AuNRs, NGO-AuNRs, and NGOHA-AuNRs were performed by inductively coupled plasma atomic emission spectrometry (ICP-AES; Thermo Electron Co.). Huh-7 cells were grown on a 100 nm dish and coincubated for 3, 12, and 24 h with AuNRs, NGO-AuNRs, and NGOHA-AuNRs, respectively. The Au concentration of the above three groups was 20 μg/mL. The cells were then washed by PBS three times, detached from the dish by trypsin, collected, counted, treated with nitric acid at 120 °C for 2 h, and kept at 70 °C overnight to ensure all AuNRs were dissolved completely. The samples were diluted to the same volume by DI water and analyzed for the total gold content by ICP-AES. The uptake efficiency was determined by the percentage of gold concentration to incubated dose per cell. To examine the competitive effect between HA and NGOHA-AuNRs-DOX to HA receptors in cellular uptake, one group of Huh-7 cells was exposed to HA polymers (1 mg/mL) and NGOHA-AuNRs-DOX (40 μg/mL) simultaneously for 12 h, while the other group was only exposed to NGOHA-AuNRs-DOX for 12 h. Then the cells of two groups were washed by PBS three times and followed the above-mentioned process for ICP-AES analysis.

Table 1. Weight Characteristics of Synthesized HA-ADH and NGO-Gold Core/Shell Nanocomposites

	mass fraction (%)		
	degree of NGO	degree of gold[a]	degree of HA[b]
HA-ADH	0	0	64.1
NGO-AuNRs	24.1	75.9	0
NGOHA-AuNRs	14.9	49.0	36.1
NGOHA	23.3	0	76.7

[a]The concentrations of gold in NGO-AuNRs and NGOHA-AuNRs were determined by TGA under O_2 flow (Figure 3d).[30] [b]The concentration of ADH in HA-ADH was determined by the ^{1}H NMR spectral data (Figure 3b).[43] The concentrations of HA in NGOHA-AuNRs and NGOHA were estimated by TGA under N_2 flow (Figure 3d, inset). [39]

The experiments were repeated three times to obtain the mean value and standard deviation.

2.8. In Vitro Chemophotothermal Therapy. To explore the synergistic effect of chemotherapy and PTT on Huh-7 cells, DOX, NGO-DOX, NGOHA-DOX, NGO-AuNRs-DOX, and NGOHA-AuNRs-DOX were administered to Huh-7 cells in 96-well plates with 0. 1 mL

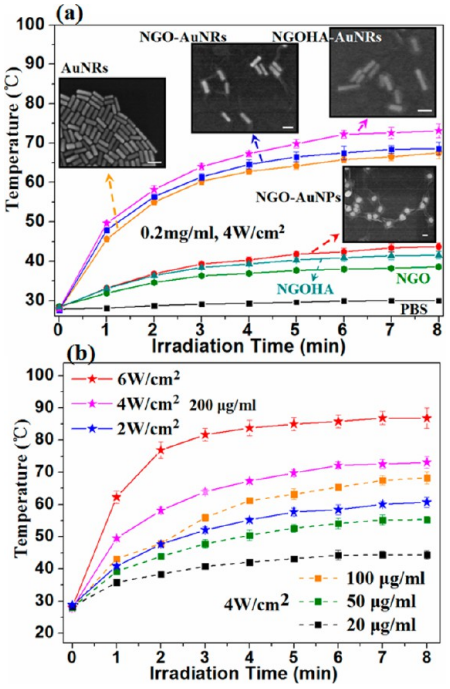

Figure 4. (a) Photothermal heating curves of NGO, NGOHA, AuNRs, NGO-AuNRs, NGO-AuNPs, and NGOHA-AuNRs at a power intensity of 4 W/cm^2. The AuNR concentration in NGO-AuNRs, NGOHA-AuNRs, and AuNRs was 0.2 mg/mL. (b) Photothermal heating curves of NGOHA-AuNRs at different power densities at a concentration of 0.2 mg/mL and photothermal heating curves of NGOHA-AuNRs at various concentrations at a power density of 4 W/cm^2. Data represent mean values for n = 3, and the bars are standard deviations for the means.

media at a density of 5000 cells/well, and each group was subdivided into groups with or without NIR laser irradiation. For PTT, samples were treated with Huh-7 cells for 4 h in 0.1 mL media, and then corresponding wells were irradiated by an 808 nm NIR laser (1 W/cm^2) for 5 min followed by further incubation for 20 h. Dead cells were stained by trypan blue and live cells by calcein and were observed by a fluorescence microscope (Olympus IX71; a green filter set was used for calcein imaging; excitation/emission = 480 nm/515 nm). For the MTT assay, samples were added in each well and incubated for 24 h. The medium was replaced by 100 μL of fresh DMEM. Then, 20 μL of a MTT solution was added and incubated for 4 h. The media were then removed, and 150 μL of DMSO was added to wells to dissolve the formazan crystals. The absorbance of each well was measured at 490 nm using a microplate reader (Thermo Multiskan MK3). The relative cell viability was calculated according to the following equation:

$$\text{relative cell viability (\%)} = 100 \times (\text{OD}_{\text{test}} - \text{OD}_0)/(\text{OD}_{\text{control}} - \text{OD}_0)$$

OD_{test} is the optical density of the cell solution under treatment, $\text{OD}_{\text{control}}$ is the optical density of the cell solution without treatment, and OD_0 is the optical density of the solution containing cells without MTT.

2.9. Targeting-Ability Evaluation in Different Cell Lines. Huh-7 and CHO cells were respectively cultured in 24-well plates at an initial density of 5 × 10_4 cells/well and incubated for 24 h in 1 mL of DMEM media. NGOHA-AuNRs-DOX or NGO-AuNRs-DOX (DOX concentration = 10 mg/mL) was then added to each cell line, respectively, with a further incubation of 12 h. For quantitative evaluation of chemotherapy or chemophotothermal therapy, each cell line treated with NGOHA-AuNRs-DOX or NGO-AuNRs-DOX (DOX concentration = 10 mg/mL) was subdivided into groups with or without NIR laser irradiation. In chemophotothermal therapy, samples were treated with Huh-7 or CHO cells for 4 h in 96-well plates, and then corresponding wells were irradiated with an 808 nm NIR laser (2 W/cm_2) for 5 min followed by further incubation for 20 h. MTT assay was performed as described above.

3. RESULTS AND DISCUSSION

3.1. Synthesis and Characterization of NGOHA-AuNRs. The synthetic strategy of NGOHA-AuNRs is shown in Figure 1. Electrostatic attraction is the main driving force for the encapsulation of positively charged CTAB-coated AuNRs in negatively charged NGO shells. HA-ADH was then conjugated to the surface of NGO-AuNRs via an amide linkage between amino groups (−NH_2) on the ADH residue and carboxylic groups (−COOH) on NGO, to afford NGOHA-AuNRs. DOX was finally loaded on NGOHA-AuNRs by $\pi-\pi$-stacking and hydrophobic interactions. In our strategy, NGOHA-AuNRs-DOX was designed for synergistic targeted chemophotothermal therapy of hepatoma Huh-7 cells.

The morphology and structure of AuNRs, NGO-AuNRs, and NGOHA-AuNRs were elucidated by SEM, TEM, and high-resolution TEM (HRTEM) measurements. The SEM and TEM images of the obtained CTAB-coated AuNRs showed that the average length and width were about 53.1 ± 8.2 and 13.8 ± 3.2 nm, respectively (about 3.8:1 aspect ratio; Figure 2a,d and S1a,d in the Supporting Information, SI). The SEM and TEM images of NGO-AuNRs (Figure 2b,e) clearly showed that they had a rough surface with one or two NGO "tails" at the ends of AuNRs, which was associated with the presence of

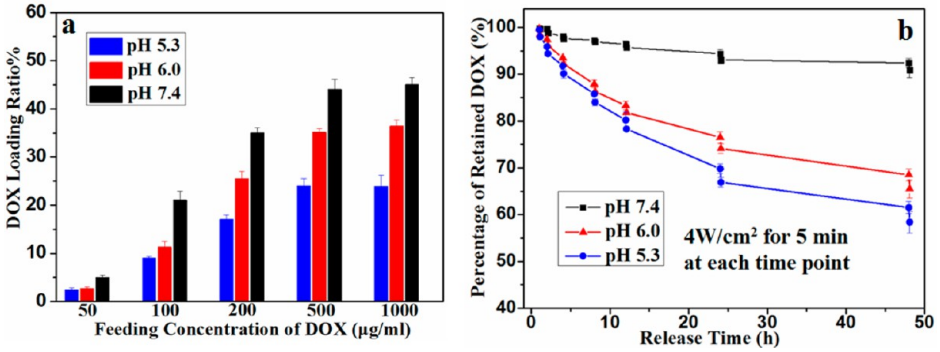

Figure 5. (a) pH-dependent DOX loading efficiency of NGOHA-AuNRs at different DOX feeding concentrations. (b) Cumulative release profiles of DOX from NGOHA-AuNRs-DOX at different pH values with 4 W/cm^2 NIR light irradiation at each time point for 5 min. Data represent mean values for n = 3, and the bars are standard deviations for the means.

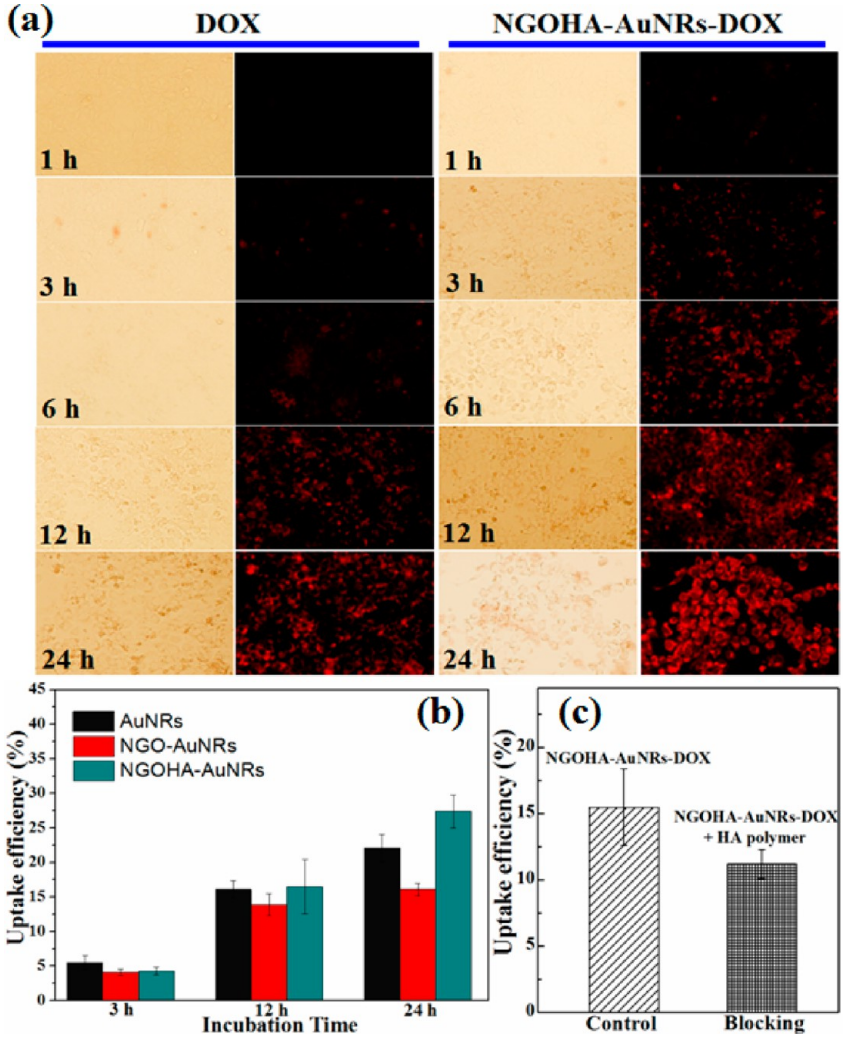

Figure 6. (a) Fluorescence microscopy images of Huh-7 cells incubated with NGOHA-AuNRs-DOX and free DOX at different incubation times. (b) Cellular uptake of AuNRs measured by ICP-AES after incubation of cells with AuNRs, NGO-AuNRs, and NGOHA-AuNRs for 3, 12, and 24 h. (c) Competitive inhibition test of HA receptors on Huh-7 cells. One group of Huh-7 cells was exposed to NGOHA-AuNRs-DOX (40 μg/mL) with HA polymers (1 mg/mL) blocking simultaneously for 12 h, while the other group was only exposed to NGOHA-AuNRs-DOX for 12 h as the control. Then the cellular uptake of AuNRs was measured by ICP-AES.

flexible and ultrathin NGO. In most cases, AuNRs were singly encapsulated in NGO shells (Figure 2b and Figure S1b,c in the SI). The thickness of the NGO shell was about 2.6 nm, as measured from HRTEM (Figure 2f). The NGO shells on the surface of AuNRs provided functional groups (−COOH) for further conjugation of HA-ADH. After HA-ADH polymer conjugation to NGO-AuNRs, the surface of NGOHA-AuNRs was blurred in the SEM image (Figure 2c).

AuNRs, NGO-AuNRs, and NGOHA-AuNRs were studied by UV−vis absorption spectroscopy (Figure 3a). The CTAB-coated AuNRs in this study exhibited two absorption bands: a strong long-wavelength band around 760 nm due to the longitudinal oscillation of electrons and a weak short-wavelength band around 520 nm due to transverse electronic oscillation.[15] The absorption peak for both NGO-AuNRs and NGOHA-AuNRs was at 239 nm, which was the characteristic absorption peak of NGO. Conjugation of the HA polymer significantly improved the absorbance of NGOHA-AuNRs and NGOHA in the NIR region and led to a solution color change (darkening) that was visible to the eyes (Figure 3a, inset).

The covalent attachment of HA to NGO-AuNRs via amide linkage was confirmed by ^{1}H NMR (Figure 3b) and FT-IR spectroscopy (Figure 3c). An ADH molecule was covalently conjugated to the HA backbone. The degree of coupling was determined by integration of the linker methylene signals (H_4) using an internal standard and the methyl resonances near 1.85−1.95 ppm of the acetamido moiety of the *N*-acetyl-D-glucosamine residue of HA.[43] NMR integration showed that 35.9% coupling of ADH to HA had occurred (Figure 3b). After conjugation of HA-ADH to NGO-AuNRs, the NMR signals of the H_4 methylene proton presented a lower intensity.[39] FT-IR spectroscopy (Figure 3c) revealed the existence of OH (3400 cm^{-1}), C═O (1733 cm^{-1}), and C═C (1580 cm^{-1}) functional groups in NGO and NGO-AuNRs. The peak at 2890 cm^{-1} in NGOHA-AuNRs was attributed to the C−H stretch from HA. The appearance of the 1685 cm^{-1} peak due to the C═O stretching of primary amide in NGOHA-AuNRs substantiated the formation of amide linkage. HA modification improved the solubility and dispersity of NGOHA-AuNRs in physiological solutions and acidic DOX solution (Figure 3f).

TGA of NGO-AuNRs and NGOHA-AuNRs under O_2 flow revealed that the weight fractions of NGO and NGOHA were 24.1% and 51.0%, respectively (Figure 3d). TGA of NGOHA-AuNRs

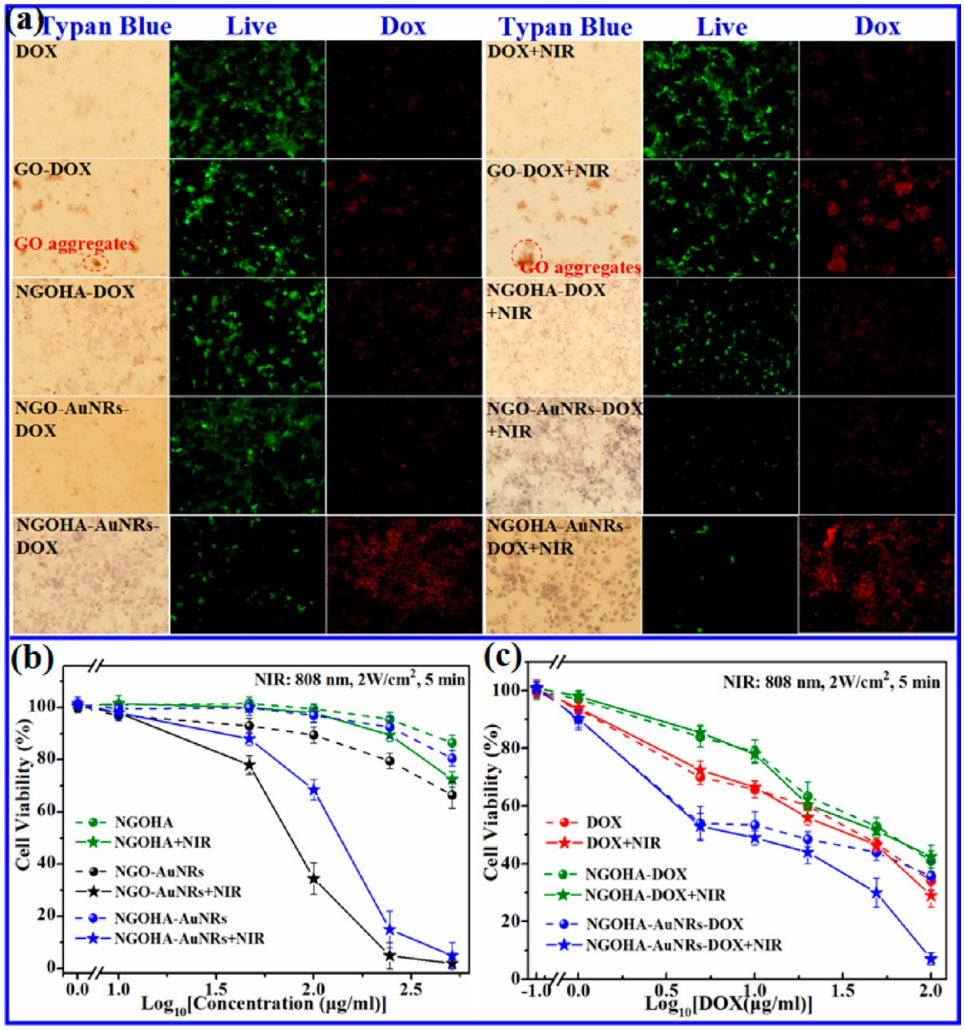

Figure 7. Cytotoxicity of hepatoma Huh-7 cells under different treatments. (a) Fluorescence microscopy images of Huh-7 cells treated with chemotherapy or chemophototherapy. The dead cells were stained with trypan blue and the live cells with calcein. (b) Cytotoxicity of NGOHA, NGO-AuNRs, and NGOHA-AuNRs to Huh-7 cells with or without NIR irradiation. (c) Cytotoxicity of NGOHA-DOX, NGOHA-AuNRs-DOX, and free DOX to Huh-7 cells with or without NIR irradiation. The relative percentage of control cells not exposed to the delivery system (nontreated) was used to represent 100% cell viability. Data represent mean values for n = 3, and the bars are standard deviations for the means.

was also performed under N_2 flow. NGOHA-AuNR nanohybrids lost their major mass in the range of 180−500 °C, mostly because of HA decomposition. According to TGA data, the approximate weight fraction of HA in NGOHA-AuNRs was about 36.1% (Table 1). The sizes and surface charges of AuNRs and NGO nanohybrids were investigated by DLS and ζ potential measurements. As shown in Figure S3 in the SI, the average hydrodynamic diameter of NGOHA-AuNRs was 139.7 nm. The initial surface charge of the CTAB-coated AuNRs was 14.9 mV (Figure 2e). After encapsulation by NGO and conjugation by HA, the surface charges of NGO-AuNRs and NGOHA-AuNRs became negative (ζ potential = −29.7 and −26.2 mV, respectively).

3.2. Photothermal Effect of NGOHA-AuNRs. Figure 4a compared the extent of the temperature rise of NGO, NGOHA, AuNRs, NGO-AuNRs, and NGOHA-AuNRs, while NGO-AuNPs[30] and PBS were used as controls. Upon irradiation by an 808 nm NIR laser at a power intensity of 4 W/cm², the NGOHA-AuNR solution temperature exceeded 60 °C within 3 min. In contrast, the bare AuNRs presented lower photothermal effects at the same AuNR concentration because the existence of NGOHA shells could further enhance the NIR absorbance. In addition, NGO-AuNPs with a spherical morphology showed much lower photothermal effects compared with NGO-AuNRs.

The photothermal effect of NGOHA-AuNRs exhibited a concentration- and laser-power-intensity-dependent manner, as shown in Figure 4b. At a high power intensity of 6 W/cm², the temperature of the NGOHA-AuNR solution at a concentration of 0.2 mg/mL could increase to 75 °C within 2 min. Therefore, it is expected that NGOHA-AuNRs would greatly improve the PTT effects on cancer cells because of the high photothermal energy conversion efficiency.

3.3. Drug Loading Capacity and NIR Light-Triggered Drug Release. The DOX loading capacity of NGOHA-AuNRs was pH-dependent, as shown in Figure 5a. The loading factor achieved 45% at pH 7.4 with a DOX feeding concentration of 0.5 mg/mL but decreased to 24% at pH 5.3. The reason was that higher pH could enhance hydrophobic interaction between DOX and NGO in NGOHA-AuNRs. Compared with folic acid-conjugated GO nanosheets as the drug carrier,[19] the DOX loading capacity of NGOHA-AuNRs was much lower because the weight fraction of NGO was only about 15% (Table 1).

The release of DOX from NGOHA-AuNRs was a slow and continuous process. At the acidic conditions, this release was

accelerated as the daunosamine group of DOX was protonated and the water solubility increased.[10] Samples of NGOHA-AuNRs-DOX dialyzed over 2 days showed that the release of DOX was 15.9% at pH 5.3 (Figure S4 in the SI). Activated release in acidic conditions could enhance the efficiency of drug delivery because both the extracellular environment of the tumor and the intracellular lysosomes and endosomes are acidic. The superior photothermal efficiency of NGOHA-AuNRs could further promote the release of DOX. Figure 5b shows that NIR irradiation enhanced the cumulative release of DOX at different time points owing to the heat-stimulative dissociation of $\pi-\pi$-stacking interactions between NGOHA-AuNRs and DOX. Upon irradiation by an NIR laser for a total time of 30 min in 24 h, the cumulative release of DOX (34.5%) was about 3.5-fold greater than that without irradiation (9.8%). The pH-sensitive and NIR-triggered release of DOX can greatly enhance the chemophotothermal therapy effects to hepatoma cells.

3.4. Cellular Uptake of NGOHA-AuNRs-DOX. The cellular uptake behavior of NGOHA-AuNRs-DOX was monitored as a function of the incubation time and compared with that of free DOX at the same DOX concentration. As shown in Figure 6a, the cellular uptake of NGOHA-AuNRs-DOX exhibited a time-dependent mode. The red fluorescence of DOX in hepatoma Huh-7 cells treated with NGOHA-AuNRs-DOX was considerably higher than that of free DOX at all time points, indicating that NGOHA-AuNRs were an efficient carriers to delivery DOX. This was possibly because NGOHA-AuNRs as stable nanosize complexes performed highly effective endocytosis in Huh-7 cells.

The cellular uptake efficiency of AuNRs, NGO-AuNRs and NGOHA-AuNRs were quantitatively measured by ICP-AES. As shown in Figure 6b, NGOHA-AuNRs exhibited the highest cell uptake capability reaching 27.4% after 24 h incubation, while NGO-AuNRs with poor dispersibility in cell medium and non-HA modification show low uptake efficiency (16.1%). To evaluate the role of HA polymers in the cellular uptake of NGOHA-AuNRs-DOX, the HA receptors were blocked by treating Huh-7 cells with excess amount of HA polymers. The results were shown in Figure 6c, the uptake efficiency of NGOHA-AuNRs-DOX significantly decreased after blocked by HA demonstrating a competitive uptake between NGOHA-AuNRs-DOX and HA. Those results suggest that HA modification of NGOHA-AuNRs could target to HA receptors on Huh-7 cells and enhance the cellular uptake.

3.5. In Vitro Chemophotothermal Therapy. In order to explore the synergistic therapeutic effect of NGOHA-AuNRs-DOX, the cell viability with different treatments was measured by both dead/live cell staining and MTT viability assays. As shown in Figure 7a, the chemotherapy and chemophotothermal synergistic therapy effects of NGOHA-AuNRs-DOX were determined by dead/live cell staining in comparison with free DOX, GO-DOX, NGOHA-DOX, and NGO-AuNRs-DOX. These qualitative results showed that NGOHA-AuNRs-DOX under NIR irradiation of 5 min at a power density of 1 W/cm^2 mediated the highest rate of cell death, and almost all of the cells were killed and stained with a blue color in the laser spot (Figures 7a and 8b). With a decrease in the power density to 0.5 W/cm^2 (Figure 8a), the energy was not high enough to kill all of the cells, and thus the blue death cell spots became much less compared with those at higher energies. DOX with low concentration (2.5 μg/mL) showed little therapeutic effect with or without NIR irradiation. GO-DOX and NGO-AuNRs-DOX without any hydrophilic modification aggregated in a cell medium and showed no chemotherapy effect, while NGO-AuNRs-DOX with NIR irradiation presented a relatively high PTT efficiency. NGOHA-DOX showed a much lower chemo-photothermal synergistic therapy effect than NGOHA-AuNRs-DOX because of the low photothermal efficiency of NGOHA.

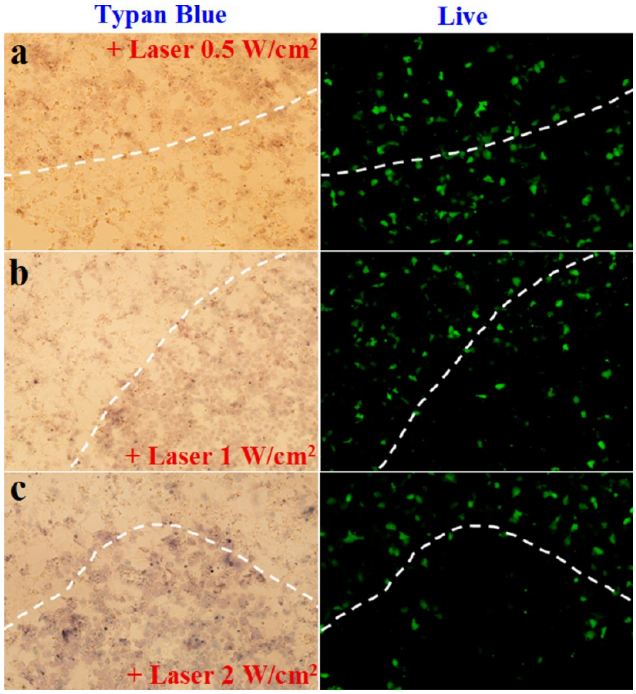

Figure 8. Fluorescence microscopy images of Huh-7 cells on the laser spot. Huh-7 cells treated with NGOHA-AuNRs-DOX exposed to NIR irradiation of (a) 0.5, (b) 1, and (c) 2 W/cm^2 power density for 5 min. The dead cells were stained with trypan blue and the live cells with calcein.

Table 2. CI Value for Combination Treatments of Hepatoma Huh-7 Cells[11]

	NGOHA-AuNRs	NGOHA-AuNRs + NIR with DOX	NGOHA-AuNRs-DOX	with DOX	with NGO-AuNRs + NIR	CI
				NGOHA-AuNRs-DOX + NIR		
IC_{50}	35.56	2.78	0.42	0.22	0.13	0.38

The results in Figure 7b indicated that our as-synthesized NGOHA-AuNRs had low cytotoxicity to Huh-7 cells. Even at a concentration of 500 μg/mL, the relative cell viability was still higher than 80%. The NGO-AuNRs with NIR irradiation showed a high PTT efficiency, and it killed 65% of the cells at a concentration of 100 μg/mL because of the high content of AuNRs (76%) compared with that in NGOHA-AuNRs (49%).

The quantitative results of chemotherapy and chemo-photothermal synergistic therapy (Figure 7c) showed that NGOHA-AuNRs-DOX killed about 56% Huh-7 cells with a little higher chemotherapy effect than free DOX (53%) at an equivalent DOX concentration of 50 μg/mL. However, with low power (1 W/cm^2) NIR irradiation for 5 min, NGOHA-AuNRs-DOX killed about 82% of the cells at the same concentration, which was about 1.5-fold and 4-fold enhanced in treatment efficacy over the separate therapeutic efficacy of chemotherapy treatment (53%) and photothermal treatment (22%; Figure 7b), respectively. The potential combination effect was evaluated by the combination index (CI) analysis in Table 2.[11]

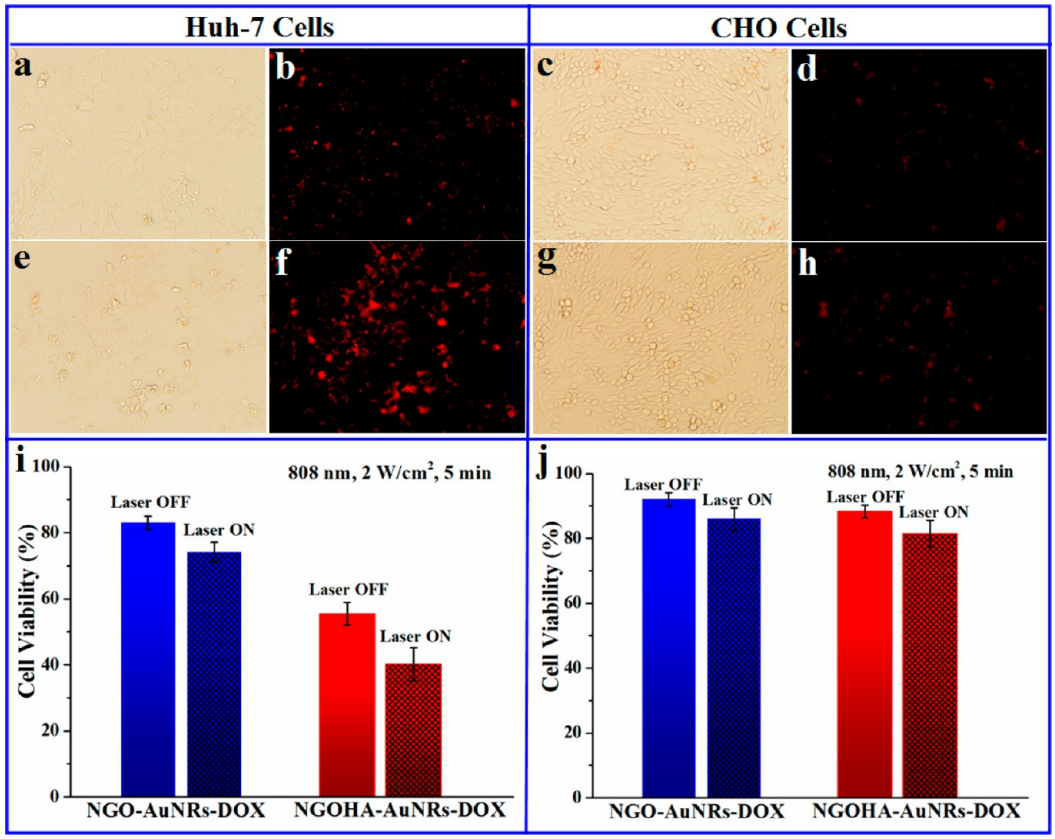

Figure 9. Targeting-ability evaluation of NGOHA-AuNRs-DOX in different cell lines. Fluorescence microscopy images of Huh-7 cells treated with NGO-AuNRs-DOX (a and b) or NGOHA-AuNRs-DOX (e and f) and images of CHO cells treated with NGO-AuNRs-DOX (c and d) or NGOHA-AuNRs-DOX (g and h). (i) Cytotoxicity of NGO-AuNRs-DOX and NGOHA-AuNRs-DOX to Huh-7 cells with or without NIR irradiation for 5 min at a power density of 2 W/cm^2. (j) Cytotoxicity of NGO-AuNRs-DOX and NGOHA-AuNRs-DOX to CHO cells with or without NIR irradiation for 5 min at a power density of 2 W/cm^2. The concentration of DOX in NGO-AuNRs-DOX and NGOHA-AuNRs-DOX was 10 μg/mL.

The CI value in this study was 0.38 (<1), which demonstrated the synergistic effect of NGOHA-AuNRs-DOX chemotherapy and PTT. The excellent synergistic therapy effect can be related to the following: (1) The NGOHA shells of AuNR enhanced the PTT efficiency. (2) Hyperthermia promoted drug release in cells. (3) NGOHA-AuNRs with a nanoscale size and HA modification improved the cellular uptake.

3.6. Targeting-Ability Evaluation of NGOHA-AuNRs-DOX in Different Cell Lines. The targeting ability of NGOHA-AuNRs-DOX was investigated in hepatoma Huh-7 cells with HA receptors and in CHO cells without HA receptors.[44] As shown in Figure 9, Huh-7 cells treated with NGOHA-AuNRs-DOX (Figure 9f) presented stronger red fluorescence than cells treated with HA-unmodified NGO-AuNRs-DOX (Figure 9b). However, CHO cells with an obviously different cellular morphology showed weaker red fluorescence in both treatments, indicating the low cellular uptake of NGOHA-AuNRs-DOX (Figure 9d) and NGO-AuNRs-DOX (Figure 9h).

For the practical application of chemophotothermal therapy, an acceptable biosafety was the most important, which requires the treatments to perform with as low a toxicity as possible to the normal or nontargeting cells. The chemotherapy and chemophotothermal therapy effects were investigated in Huh-7 and CHO cells, as shown in Figure 9i,j. Both chemotherapy and chemophotothermal therapy showed little therapeutic efficacy to CHO cells with a cell viability higher than 80%, while in the same treatment conditions, the cell viability of Huh-7 was only 40%. These results highlighted the low toxicity and side effects to nontargeting cells in chemophotothermal treatment by NGOHA-AuNRs-DOX, with excellent therapy efficacy to the targeting cells simultaneously.

4. CONCLUSIONS

In summary, novel, multifunctional, and low-toxicity NGOHA-AuNR nanocomposites have been developed to serve as a targeting synergistic chemophotothermal therapy agent for hepatoma Huh-7 cells. They exhibited high photothermal energy conversion efficiency and pH-sensitive, NIR-triggered drug release characteristics. The HA modification of NGOHA-AuNRs not only enhanced the solubility in physiological conditions but also offered the capability of targeting Huh-7 cells. The comparison study of the therapeutic efficacy in different cell lines demonstrated that NGOHA-AuNRs-DOX presented significantly synergistic chemophotothermal therapy effects that were about 1.5-fold and 4-fold higher than that of separate chemotherapy and photothermal treatment to targeting cells, respectively, and with biosafety and low side effects to nontargeting cells at the same time. Furthermore, our strategy could be extended to the construction of other NGO-encapsulated functional nanomaterials for the synergistic therapy of tumors.

■ ASSOCIATED CONTENT

Supporting Information

Description related to the SEM images of AuNRs and NGO-AuNRs and analysis of the average length and width of AuNRs (Figure S1), UV−vis spectra of NGOHA-AuNRs-DOX (Figure S2), average

hydrodynamic diameter of GO, NGO, NGO-AuNRs, and NGOHA-AuNRs (Figure S3), and cumulative release profiles of DOX from NGOHA-AuNRs at different pH values (Figure S4). This material is available free of charge via the Internet at http://pubs.acs.org.

AUTHOR INFORMATION

Corresponding Authors

*E-mail: liqiuhong2004@hotmail.com. Tel./fax: +86-0731-88664019.

*E-mail: zhuhaizhen69@yahoo.com. Tel./fax: +86-0731-88664019.

*E-mail: thwang@aphy.iphy.ac.cn. Tel./fax: +86-0731-88664019.

Notes

The authors declare no competing financial interest.

ACKNOWLEDGMENTS

We are thankful for financial support from the National Natural Science Foundation of China (Grant 21003041), the Specialized Research Fund for the Doctoral Program of Higher Education of China (Grant 20120161110016), and the Hunan Provincial Natural Science Foundation of China (Grant 11JJ7004).

REFERENCES

(1) Zhang, Z. J.; Wang, J.; Chen, C. Y. *Adv. Mater.* **2013**, *25*, 3869−3880.

(2) Gao, L.; Fei, J. B.; Zhao, J.; Li, H.; Cui, Y.; Li, J. B. *ACS Nano* **2012**, *6*, 8030−8040.

(3) Sherlock, S. P.; Tabakamn, S. M.; Xie, L. M.; Dai, H. J. *ACS Nano* **2011**, *5*, 1505−1512.

(4) Zhang, K.; Hao, L. L.; Hurst, S. J.; Mirkin, C. A. *J. Am. Chem. Soc.* **2012**, *134*, 16488−16491.

(5) Cutler, J. I.; Auyeung, E.; Mirkin, C. A. *J. Am. Chem. Soc.* **2012**, *134*, 1376−1391.

(6) Hu, S. H.; Chen, Y. W.; Hung, W. T.; Chen, I. W.; Chen, S. Y. *Adv. Mater.* **2012**, *24*, 1748−1754.

(7) Chen, M. L.; He, Y. J.; Chen, X. W.; Wang, J. H. *Bioconjugate Chem.* **2013**, *24*, 387−397.

(8) Moon, H. K.; Lee, S. H.; Choi, H. C. *ACS Nano* **2009**, *3*, 3707−3713.

(9) Shi, X. Z.; Gong, H.; Li, Y. J.; Wang, C.; Cheng, L.; Liu, Z. *Biomaterials* **2013**, *34*, 4786−4793.

(10) Wang, Y.; Wang, K. Y.; Zhao, J. F.; Liu, X. G.; Bu, J.; Yan, X. Y.; Huang, R. Q. *J. Am. Chem. Soc.* **2013**, *135*, 4799−4804.

(11) Liu, S. H.; Guo, Y. B.; Huang, R. Q.; Li, J. F.; Huang, S. X.; Kuang, Y. Y.; Han, L.; Jiang, C. *Biomaterials* **2012**, *33*, 4907−4916.

(12) Robinson, J. T.; Tabakman, S. M.; Liang, Y. Y.; Wang, H. L.; Casalongue, H. S.; Vinh, D.; Dai, H. J. *J. Am. Chem. Soc.* **2011**, *133*, 6825−6831.

(13) Dickerson, E. B.; Dreaden, E. C.; Huang, X. H.; El-Sayed, I. H.; Chu, H. H.; Pushpanketh, S.; McDonald, J. F.; El-Sayed, M. A. *Cancer Lett.* **2008**, *269*, 57−66.

(14) Gole, A.; Murphy, C. J. *Chem. Mater.* **2004**, *16*, 3633−3640.

(15) Huang, X. H.; EI-Sayed, I. H.; Qian, W.; EI-Sayed, M. A. *J. Am. Chem. Soc.* **2006**, *128*, 2115−2120.

(16) Huang, P.; Bao, L.; Zhang, C. L.; Lin, J.; Luo, T.; Yang, D. P.; He, M.; Li, Z. M.; Gao, G.; Gao, B.; Fu, S.; Cui, D. X. *Biomaterials* **2011**, *32*, 9796−9809.

(17) Shen, S.; Tan, H. Y.; Zhang, X. T.; Ren, J. F.; Pang, Z. Q.; Wang, D. G.; Gao, H. L.; Qian, Y.; Jiang, X. G.; Yang, W. L. *Biomaterials* **2013**, *34*, 3150−3158.

(18) Niidome, T.; Yamagata, M.; Okamoto, Y.; Akiyama, Y.; Takahashi, H.; Kawano, T.; Katayama, Y.; Niidome, Y. *J. Controlled Release* **2006**, *114*, 343−347.

(19) Zhang, L. M.; Lu, Z. X.; Zhao, Q. H.; Huang, J.; Shen, H.; Zhang, Z. J. *Small* **2011**, *7*, 460−464.

(20) Bao, H. Q.; Pan, Y. Z.; Ping, Y.; Sahoo, N. G.; Wu, T. F.; Li, L.; Li, J.; Gan, L. H. *Small* **2011**, *7*, 1569−1578.

(21) Kim, H.; Kim, W. J. *Small* **2013**, DOI: 10.1002/smll.201202636.

(22) Shen, H.; Liu, M.; He, H. X.; Zhang, L. M.; Huang, J.; Chong, Y.; Dai, J. W.; Zhang, Z. J. *ACS Appl. Mater. Interfaces* **2012**, *4*, 6317−6323.

(23) Sun, X. M.; Liu, Z.; Welsher, K.; Robinson, J. T.; Goodwin, A.; Zaric, S.; Dai, H. J. *Nano Res.* **2008**, *1*, 203−212.

(24) Zhang, X. Y.; Yin, J. L.; Peng, C.; Hu, W. Q.; Zhu, Z. Y.; Li, W. X.; Fan, C. H.; Huang, Q. *Carbon* **2011**, *49*, 986−995.

(25) Lu, B. A.; Li, T.; Zhao, H. T.; Li, X. D.; Gao, C. T.; Zhang, S. X.; Xie, E. Q. *Nanosale* **2012**, *4*, 2978−2982.

(26) Yang, K.; Feng, L. Z.; Shi, X. Z.; Liu, Z. *Chem. Soc. Rev.* **2013**, *42*, 530−547.

(27) Yang, K.; Li, Y. J.; Tan, X. F.; Peng, R.; Liu, Z. *Small* **2013**, *9*, 1492−1503.

(28) Sreejith, S.; Ma, X.; Zhao, Y. L. *J. Am. Chem. Soc.* **2012**, *134*, 17346−17349.

(29) Chen, Y. T.; Guo, F.; Hu, H.; Kulaots, I.; Walsh, E.; Hurt, H. R. *ACS Nano* **2013**, *7*, 3744−3753.

(30) Xu, C.; Yang, D. R.; Mei, L.; Lu, B. A.; Chen, L. B.; Li, Q. H.; Zhu, H. Z.; Wang, T. H. *ACS Appl. Mater. Interfaces* **2013**, *5*, 2715−2724.

(31) Xu, L. G.; Liu, Y.; Chen, Z. Y.; Li, W.; Liu, Y.; Wang, L. M.; Liu, Y.; Wu, X. C.; Ji, Y. L.; Zhao, Y. L.; Ma, L. Y.; Shao, Y. M.; Chen, C. Y. *Nano Lett.* **2012**, *12*, 2003−2012.

(32) Sahu, A.; Choi, W. I.; Lee, J. H.; Tae, G. *Biomaterials* **2013**, *34*, 6239−6248.

(33) Zhang, W.; Guo, Z. Y.; Huang, D. Q.; Liu, Z. M.; Guo, X.; Zhong, H. Q. *Biomaterials* **2011**, *32*, 8555−8561.

(34) Zedan, A. F.; Moussa, S.; Terner, J.; Atkinson, G.; El-Shall, M. S. *ACS Nano* **2013**, *7*, 627−636.

(35) Lim, D. K.; Barhoumi, A.; Wylie, R. G.; Reznor, G.; Langer, R. S.; Kohane, D. S. *Nano Lett.* **2013**, *13*, 4075−4079.

(36) Oh, E. J.; Park, K.; Kim, K. S.; Kim, J.; Yang, J. A.; Kong, J. H.; Lee, M. Y.; Hoffman, A. S.; Hahn, S. K. *J. Controlled Release* **2010**, *141*, 2−12.

(37) Kim, K. S.; Hur, W.; Park, S. J.; Hong, S. W.; Choi, J. E.; Goh, E. J.; Yoon, S. K.; Hahn, S. K. *ACS Nano* **2010**, *4*, 3005−3014.

(38) Lee, M. Y.; Yang, J. A.; Jung, H. S.; Beack, S.; Choi, J. E.; Hur, W.; Koo, H.; Kim, K.; Yoon, S. K.; Hahn, S. K. *ACS Nano* **2012**, *6*, 9522−9531.

(39) Li, F. Y.; Park, S. J.; Ling, D. S.; Park, W.; Han, J. Y.; Na, K.; Char, K. *J. Mater. Chem. B* **2013**, *1*, 1678−1686.

(40) Marcano, D. C.; Kosynkin, D. V.; Berlin, J. M.; Sinitskii, A.; Sun, Z. Z.; Slesarev, A.; Alemany, L. B.; Lu, W.; Tour, J. M. *ACS Nano* **2010**, *4*, 4806−4814.

(41) Wang, Y.; Li, Z. H.; Hu, D. H.; Lin, C. T.; Li, J. H.; Lin, Y. H. *J. Am. Chem. Soc.* **2010**, *132*, 9274−9276.

(42) Yang, D. R.; Xue, B. B.; Wang, X. H.; Yu, X. Y.; Niu, N. L.; Gao, Y. M.; Liu, C.; Zhu, H. Z. *PloS One* **2013**, *8*, e64932.

(43) Pouyani, T.; Prestwich, G. D. *Bioconjugate Chem.* **1994**, *5*, 339−347.

(44) Zheng, Z.; Cummings, R. D.; Pummill, P. E.; Kincade, P. K. *J. Clin. Invest.* **1997**, *100*, 1217−1229.